Characterization of collector optic material samples before and after exposure in LPP and DPP EUV sources

Huatan Qiu[a], Darren A. Alman[a], Keith C. Thompson[a], Matthew D. Coventry[a], Joshua B. Spencer[a], Matthew R. Hendricks[a], Erik L. Antonsen[a], Brian E. Jurczyk[a], David N. Ruzic[a], Tim P. Spila[b], Ginger Edwards[c], Stefan Wurm[c], Obert Wood[c], Robert Bristol[d]

[a] Plasma-Material Interaction Group, University of Illinois at Urbana-Champaign, IL USA 61801

[b] Center for Microanalysis of Materials, University of Illinois at Urbana-Champaign, IL USA 61801

[c] SEMATECH, Austin, TX USA 78741

[d] Intel Components Research, Hillsboro, OR USA 93751

ABSTRACT

The University of Illinois at Urbana-Champaign (UIUC) and several national laboratories are collaborating on an SEMATECH effort to characterize xenon plasma exposure effects on EUV condenser optics. A series of mirror samples provided by SEMATECH were exposed for 10M shots in an Xtreme Technologies XTS 13-35 commercial EUV discharge plasma source at UIUC and 5M at the high-power TRW laser plasma source at Sandia National Laboratories. Results for both pre and post-exposure material characterization are presented, for samples exposed in both facilities. Surface analysis performed by the Center for Microanalysis of Materials at UIUC investigates mirror degradation mechanisms by measuring changes in surface roughness, texture, and grain sizes as well as analysis of implantation of energetic Xe ions, Xe diffusion, and mixing of multilayers. Materials characterization on samples removed after varying exposure times in the XTS source, together with in-situ EUV reflectivity measurements, identify the onset of different degradation mechanisms within each sample over 1M-100M shots. Results for DPP-exposed samples for 10 million shots in our XCEED (Xtreme Commercial EUV Exposure Device) experiment showed, in general, that samples were eroded and the surfaces were roughened with little change to the texture. AFM results showed an increase in roughness by a factor of 2-5 times, with two exceptions. This was confirmed by x-ray reflectivity (XRR) data, which showed similar roughening characteristics and also confirmed the smoothening of two samples. SEM pictures showed that erosion was from 4-47 nm, depending on the sample material and angle of incidence for debris ions. Finally, microanalysis of the exposed samples indicated that electrode material was implanted at varying depths in the samples. The erosion mechanism is explored using a spherical sector energy analyzer (ESA) to measure ion species and their energy spectra. Energy spectra for ions derived from various chamber sources are measured as a function of the Argon flow rate and angle from the centerline of the pinch. Results show creation of high energy ions (up to E = 13 keV). Species noted include ions of Xe, the buffer gas, and various electrode materials. The bulk of fast ion ejection from the pinch includes Xe^{+} which maximizes at ~8 keV followed by Xe^{2+} which maximizes at ~5 keV. Data from samples analysis and ESA measurements combined indicate mechanism and effect for debris-optic interactions and detail the effectiveness of the current debris mitigation schemes.

1 . INTRODUCTION

This paper reports on part of the Collector Lifetime and Erosion Project at the University of Illinois at Urbana-Champaign, sponsored by SEMATECH and operated in cooperation with Intel Corporation and Xtreme Technologies GmbH. The purpose of this project is to examine the effects of ion debris interaction with the primary collector optic in commercial EUV sources to ascertain the fundamental erosion processes and critical lifetime issues facing high-volume manufacturing for EUV lithography.

This report covers the comparative surface analysis between optically exposed samples at the SNL LPP experimental facility and the UIUC DPP experimental facility.

Emerging Lithographic Technologies IX, edited by R. Scott Mackay,
Proceedings of SPIE Vol. 5751 (SPIE, Bellingham, WA, 2005)
0277-786X/05/$15 · doi: 10.1117/12.600093

1.1. Experimental exposure

The seven samples investigated consist of one Si/Mo multilayer mirror (MLM) and six single material films of thickness ~200 nm deposited on Si substrates. The multilayer, named "ML1", is optimized for 5° operation with 50 bilayer pairs with a period thickness of 6.95 nm and a gamma of 0.4, and has a 2.3 nm Ru capping layer. The seven single films are C, Au, Mo, Pd, Ru, and Si. The MLM and single films were all prepared by Saša Bajt at Lawrence Livermore National Laboratory.

The samples were exposed to 500,000 shots in the ETS LPP source at SNL. This number is less than the 10 million shots for the DPP exposures, because of problems with the xenon filament nozzle. Some of the differences seen between the two batches of exposed samples could be explained by the unequal lengths of exposures. However the samples were closer to the source in the LPP and, unlike the DPP exposures, there was no debris mitigation in the LPP exposures – perhaps lessening the effect of exposure length.

2. RESULTS AND DISCUSSION

2.1. Surface roughness

Surface roughness can limit reflectivity of surfaces, particularly in the case of a grazing incidence collector. To investigate how the exposures affected the samples in this regard, atomic force microscopy (AFM) was used to measure surface height variations over several different lateral length scales. Scans were done over 5x5, 2x2, 1x1, and 0.5x0.5 μm^2 areas. Examples are shown in Figure 1-Figure 4 are 2x2 μm^2 AFM scans of the seven samples before and after exposure in the LPP source.

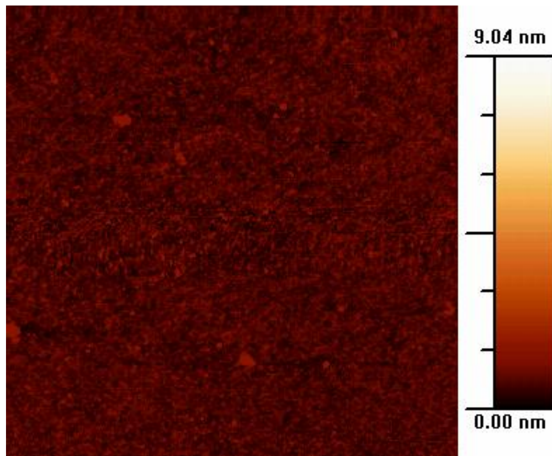

Figure 1. AFM 2 µm x 2 µm scan of the unexposed ML1 sample

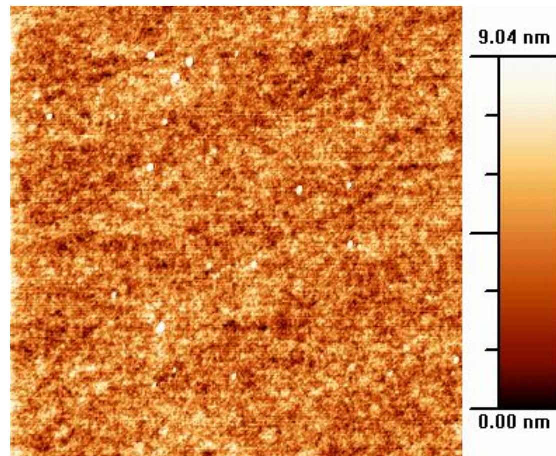

Figure 2. AFM 2 µm x 2 µm scan of the LPP-exposed ML1 sample

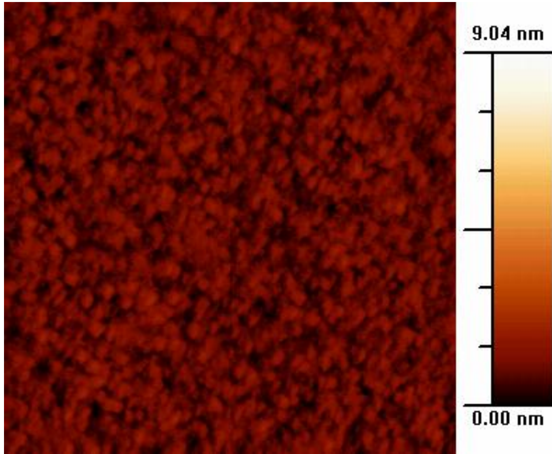

Figure 3. AFM 2 µm x 2 µm scan of the unexposed Mo sample

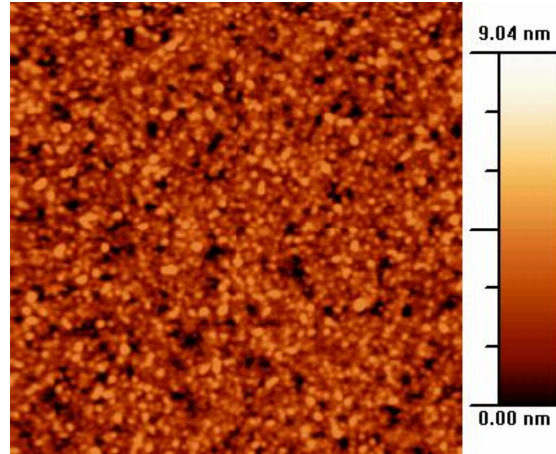

Figure 4. AFM 2 µm x 2 µm scan of the LPP-exposed Mo sample

Several samples (e.g. Au, Si) show a clear increase in visual roughness. When analyzed by computer we can calculate the RMS roughness, which is the most commonly quoted roughness parameter. Table 1 summarizes the AFM results, giving the calculated RMS roughness values for each of the seven samples. In all but one case, the roughness values increased by a factor of between 1.1x and 4.5x. The metallic films Au, Mo, Ru, and Pd showed the most dramatic increases in roughness, followed by Si and C. The multilayer mirror actually became slightly smoother after exposure, which is perhaps an unexpected result. It is possible that if the top Ru surface that is relatively rough were eroded, the underlying Si layer would be significantly smoother. Indeed, this is a possibility due to the erosion measurements presented in Section 2.3.

Table 1. AFM Results for Unexposed, LPP-exposed, and DPP-exposed samples

	RMS Roughness (nm)			
Sample	Pre-exposure	LPP-exposed	Change (exp/un-exp)	DPP-exposed
Au	0.49	2.22	4.5	1.55
C	0.14	0.16	1.1	0.86
ML1	0.32	0.25	0.8	0.13
Mo	0.33	1.04	3.2	0.76
Pd	0.63	1.07	1.7	1.28
Ru	0.27	0.58	2.1	0.80
Si	0.09	0.16	1.8	0.26

X-ray reflectivity (XRR) measurements can give information on film thicknesses, interfaces, and roughness by measuring the intensity of reflected x-rays vs. angle. Interfaces show up as interference patterns in the trace of reflectivity vs. angle. The thickness of layers can be deduced from the period in the peaks that come about from interference off of different interfaces. The roughness can be determined from the fall off of reflectivity beyond the critical angle. Theoretically, reflectivity should fall off as θ^{-4} according to the Fresnel equation. A faster fall off would indicate surface roughness. Because this is an indirect measurement of roughness based on fitting data to a model, it is not as good a measurement as the AFM results shown in Table 1. However, XRR does confirm some of the trends. For example; Au, Mo, Pd, and Ru are definitely more rough than Si and C. The DPP-exposed surfaces also appear to be rougher than their LPP counterparts. Figure 5 and Figure 6 detail the XRR data for ML1 and Mo.

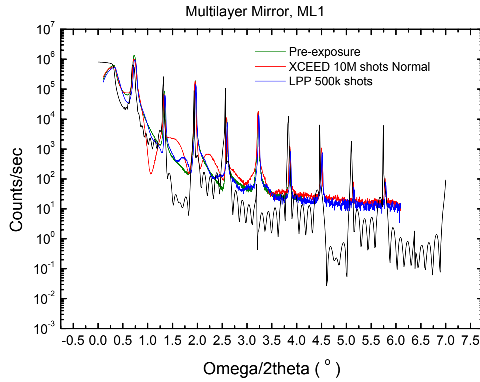

Figure 5. XRR data and theoretical curve for ML1

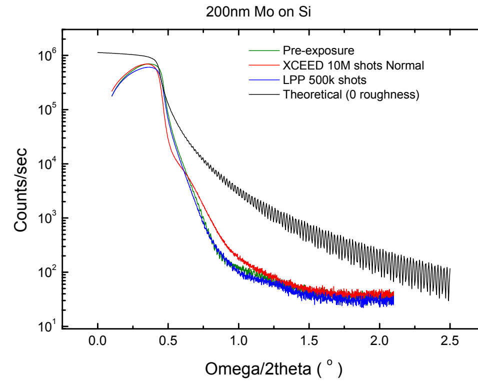

Figure 6. XRR data and theoretical curve for Mo

The roughness values obtained by fitting the XRR data to theory are shown in Table 2. It is not clear whether the LPP-exposed samples are rougher than the unexposed samples. However, they are clearly not as rough as the DPP-exposed samples.

Table 2. XRR Results for Unexposed, LPP-exposed, and DPP-exposed samples

	RMS Roughness (nm)			
Sample	Pre-exposure	LPP-exposed	Change (exp/un-exp)	DPP-exposed
Au	1.11	0.99	0.9	1.79
C	0.79	0.33	0.4	9.20
ML1	0.25	—	—	0.15
Mo	1.70	1.43	0.8	2.00
Pd	1.26	0.82	0.7	1.14
Ru	0.31	0.74	2.4	0.98
Si	0.001	0.001	1.0	N/A

2.2. Sample texture

Measurements of the preferred orientation of crystallites, or texture, of the samples were made using x-ray diffraction (XRD). Several different types of scans were performed. A $\theta - 2\theta$ scan uses a symmetrical geometry where the angle between the surface plane and x-ray source (ω) is equal to the angle between the surface plane and the x-ray detector (θ). A scan over a range of angles with ω and θ coupled, while recording the diffracted intensity gives the overall crystallinity of the sample as well as the out-of-plane lattice spacing. The intensity peaks in the out-of-plane lattice spacing show which crystal orientations are present in the sample. The results of the $\theta - 2\theta$ scans are shown in Figure 7 and Figure 8. In all cases, the films are grown on a (100) Si substrate, so no other peaks could be seen around the dominant peak from the substrate between 60° and 70°. This also made it impossible to learn much from the Si film. The C film did not show any peaks in the $\theta - 2\theta$ scan. This means the C film is either too thin or amorphous. In the cases that did give good data, all samples showed a strong preference for one orientation as evidenced by relative peak heights significantly different than would be expected in an untextured sample of the same material. Au, Mo, Pd, and Ru favored the (111), (110), (111), and (002) orientations, respectively. These results are summarized in Table 3.

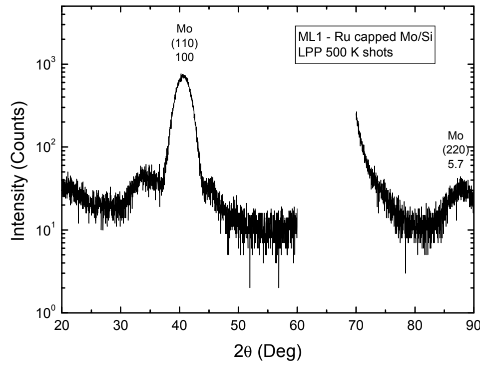

Figure 7. θ-2θ scan of the LPP-exposed ML1 sample

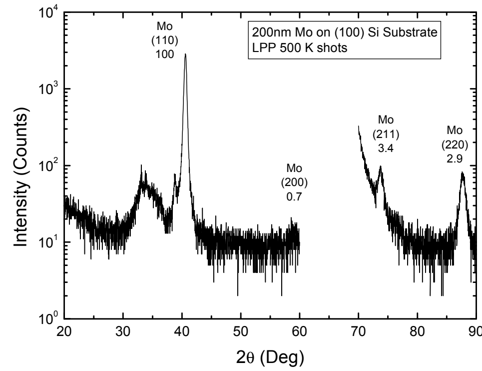

Figure 8. θ-2θ scan of the LPP-exposed Mo sample

Table 3. X-ray diffraction θ-2θ peaks, normalized to the largest peak that would be found in an untextured sample.

			Normalized Peak Height			FWHM of Rocking Curve (°)	
Sample	2θ (°)	h k l	Untextured	Pre-exp.	LPP-exp.	Pre-exp.	LPP-exp.
Au	38.185	1 1 1	100	100.0	100.0	5.78	5.84
	44.393	2 0 0	52	0.0	0.0	—	—
	77.549	3 1 1	36	0.1	0.1	—	—
	81.724	2 2 2	12	2.4	3.9	—	—
Mo in MLM	40.550	1 1 0	100	100.0	100.0	13.1	13.3
	58.661	2 0 0	16	0.0	0.0	—	—
	73.753	2 1 1	31	0.0	0.0	—	—
	87.687	2 2 0	9	3.3	5.7	—	—
Mo	40.550	1 1 0	100	100.0	100.0	12.3	12.5
	58.661	2 0 0	16	0.7	0.7	—	—
	73.753	2 1 1	31	2.3	3.4	—	—
	87.687	2 2 0	9	1.7	2.9	—	—
Pd	40.119	1 1 1	100	100.0	100.0	8.44	8.59
	46.659	2 0 0	60	0.5	0.6	—	—
	82.100	3 1 1	55	0.5	1.0	—	—
	86.619	2 2 2	15	1.5	2.9	—	—
Ru	38.420	1 0 0	40	29.0	30.1	—	—
	42.189	0 0 2	35	797.0	806.8	9.53	9.46
	44.044	1 0 1	100	100.0	100.0	—	—
	78.465	1 0 3	25	2.0	3.3	—	—
	82.305	2 0 0	6	0.0	0.0	—	—
	84.790	1 1 2	25	2.5	5.1	—	—
	86.046	2 0 1	20	3.7	7.5	—	—

A rocking curve can show how strongly orientations are preferred. This is a scan where ω is varied with a fixed 2θ angle. The intensity curve will form a Gaussian peak, with the broadness of the peak giving an indication of the overall crystalline quality of the film and how strongly the orientation is preferred. For example, a single crystal film would have a very narrow peak, because as soon as the ω angle were moved the smallest amount, the condition for reflection would be broken. Conversely for completely random orientations (no preference for any orientation over the others), as ω is

varied there would always be the same number of crystallites able to reflect the x-rays – resulting in a flat rocking curve. Rocking curves were performed on the dominant peak in each sample's $\theta - 2\theta$ scan. The results are also shown in Table 3.

The broadness of the peaks in the $\theta - 2\theta$ scan can give the grain size in the direction normal to the surface, by measuring the full width at half maximum (FWHM) of the peak and using the Scherrer equation. The results are shown for samples that had well defined peaks in the $\theta - 2\theta$ scans. The grain size generally decreased after exposure, and the decrease was more pronounced than in the DPP exposures. This is consistent with a higher fluence of damaging ions over the DPP exposures.

Table 4. Grain size calculations for Au, Mo, Pd, and Ru samples

			Grain size (nm)		
Sample	2θ (°)	h k l	Pre-exp.	LPP-exp.	DPP-exp.
Au	38.185	1 1 1	351	316	367
Mo	40.550	1 1 0	243	228	241
Pd	40.119	1 1 1	368	334	352
Ru	42.189	0 0 2	324	300	317

A pole figure is a texture measurement done by rotating the sample about its surface normal (φ) and tilting the sample about its axis parallel to the direction of the x-rays (ψ). The source (ω) and detector (θ) angles are fixed to look at a particular orientation of planes. Pole figures can give the preferred orientation and tell whether the sample is single or poly crystalline. Most of the metallic films exhibited a fiber texture, with many grains favoring a particular orientation but all with different rotations in the plane of the sample. These films grow in columns extending vertically up from the substrate. A columnar structure like this could affect the diffusion and transport of particles in the film, for example. Diffusion would be much faster in the direction normal to the surface than in a direction parallel to the surface in these samples.

As an example of the fiber texture, Figure 9 clearly shows that the Au sample exhibits a fiber texture favoring the (111) direction. The (111) orientation is seen as a strong peak in the center of the (111) pole figure. The (111) direction is also seen in the (200) pole figure as the ring positioned 54° out from the center (in the ψ direction). The fact that the ring is uniform as the sample is rotated in the φ direction shows that it is not a single crystal.

A single crystal would show four discrete peaks separated by 90° in φ rather than a ring. A perfect example of a single crystal is shown in Figure 10 for Si. Here the preferred (100) direction appears as four discrete peaks separated by 90° in the (220) pole figure. This suggests that the Si film grown on the Si substrate is either too thin and the signal is dominated by the substrate in these XRD measurements, or that it grew epitaxially. The latter is more likely, since the film should be ~200 nm thick.

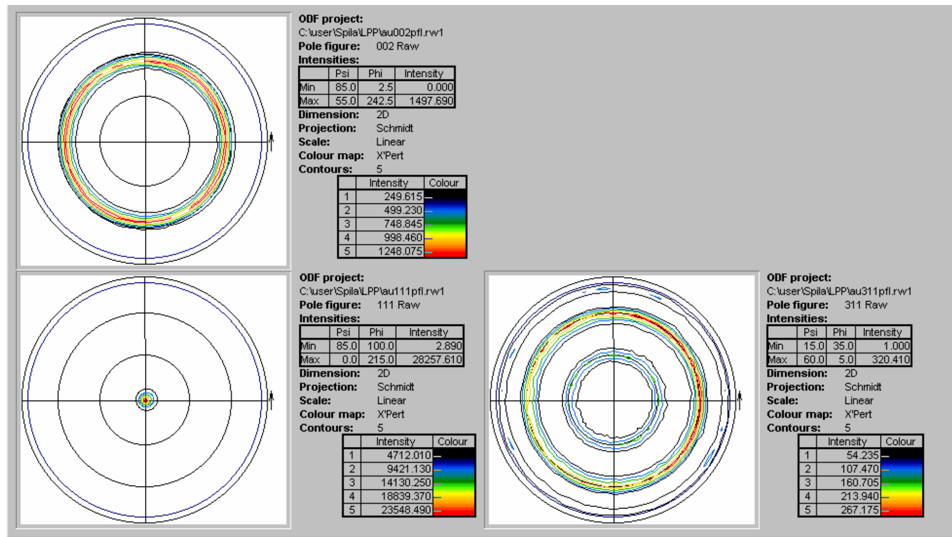

Figure 9. (002), (111), and (311) pole figures for the LPP-exposed Au sample.

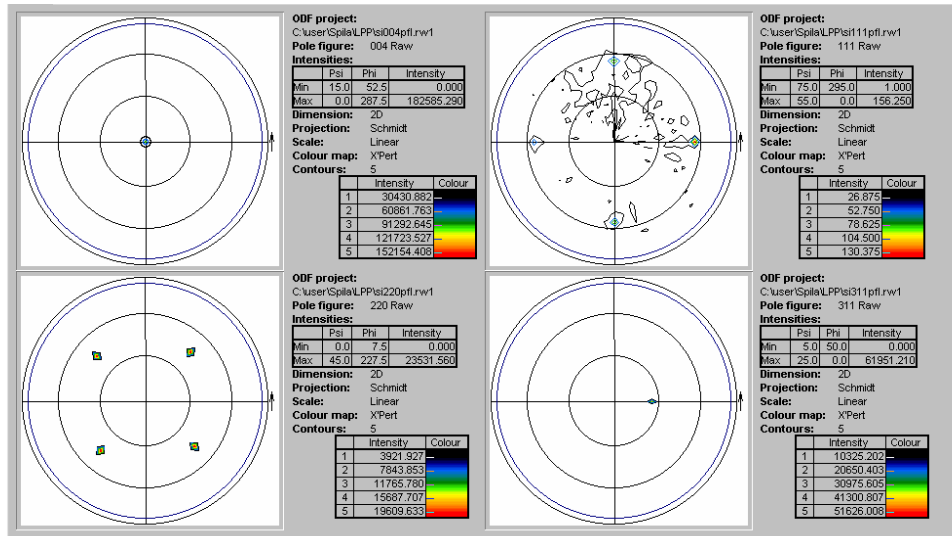

Figure 10. (004), (220), (111), and (311) pole figures for the LPP-exposed Si sample.

2.3. Erosion

In theory, thickness estimates can be obtained by depth profiles in a technique like Auger Electron Spectroscopy (AES). If the depth profile is performed by sputtering all the way through the film into the substrate, the amount of sputtering required to reach the substrate gives the film thickness. In practice, however, the sputtering rate was found to vary too much in the AES instrument and such thickness estimates were not reliable. For the multilayer mirror, however, AES is able to confirm that there are 50 Si and Mo layers (see Figure 13).

The best measurements of thickness that we obtained were from cross sectional scanning electron microscopy (SEM). Figure 11 and Figure 12 show film cross sections for two of the samples after exposure in the LPP source. Table 5

summarizes the thickness measurements derived from the cross sections. When compared to thickness estimates made on the unexposed samples, erosion of between 5 and 48 nm was seen. This is generally less than the erosion seen in the DPP exposures (except for Pd), which is logical because the number of shots was 20x less in the LPP exposures.

Several samples were difficult or impossible to measure. The measurement of the Ru sample before exposure is questionable because the film seemed to have delaminated in the cross-sectional view. The C and Si samples often did not provide enough contrast to clearly identify the film-substrate. We were fortunate to get a good C cross section for the LPP-exposed sample, but had nothing to compare it to from the unexposed or DPP-exposed batches.

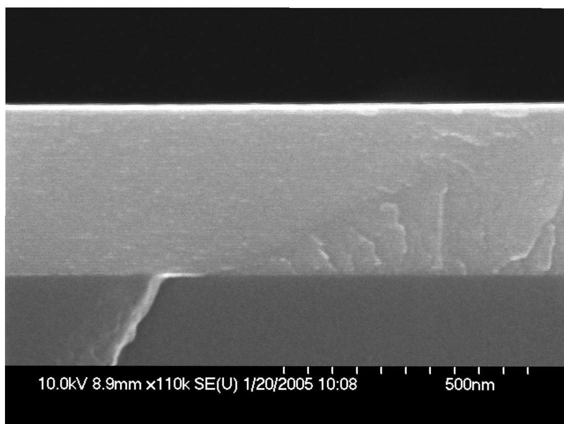

Figure 11. SEM image of the LPP-exposed ML1 sample

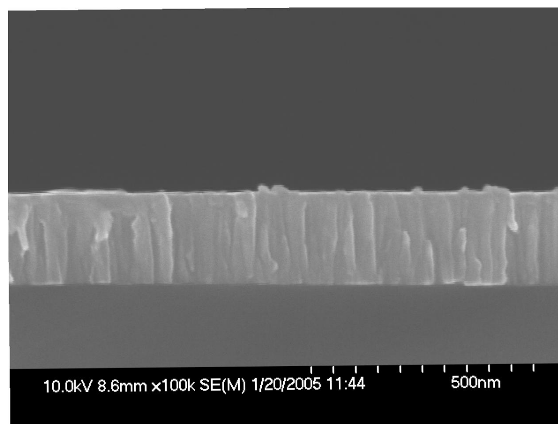

Figure 12. SEM image of the LPP-exposed Mo sample

There are several possible reasons for differences in amounts of erosion between the LPP and DPP exposures. The LPP samples were exposed to 500,000 shots vs. 10 million for the DPP exposures. However, there is clearly not 20 times less erosion seen in the LPP samples. We can conclude from this that the erosive ion flux on the samples exposed to the LPP source was much higher than the flux on the samples exposed to the DPP source. It is possible that some of this is due to the difference between LPP & DPP sources. However, certainly some of it is attributable to the distance from the source to the samples. The samples were only 10-17 cm from the source in the LPP exposures, but were 56 cm from the pinch in the DPP exposures. The LPP exposures also had no debris mitigation.

Table 5. SEM thickness measurements for pre-exposure and LPP-exposed samples. Net erosion figures are shown for LPP and previous DPP exposures for comparison

	Thickness (nm)			
Sample	Pre-exp.	LPP-exp.	Erosion	DPP erosion
Au	219	205	14	54
C	—	112	—	—
ML1	355	350	5	13
Mo	219	211	8	10
Pd	278	230	48	20
Ru	186	209	-23	-14
Si	—	—	—	—

2.4. Composition

Both AES and x-ray photoelectron spectroscopy (XPS) were used to investigate the film composition before and after exposure. Both can give the atomic concentration of a sample very near the surface by measuring the kinetic energy of ejected electrons. Some elements are more sensitive to either AES or XPS, so it is useful to use both techniques. Our

XPS instrument also had problems of late and could not do any depth profiling (taking atomic concentration data while simultaneously removing material from the sample by sputtering with Ar) due to a problem pumping Ar. In AES, we were able to sputter all the way through the samples.

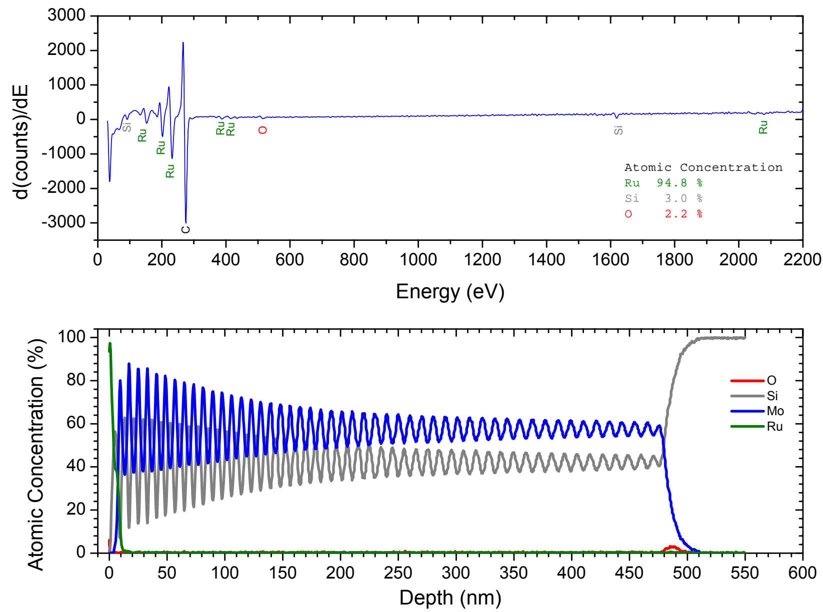

Figure 13. AES data for the LPP-exposed ML1 sample

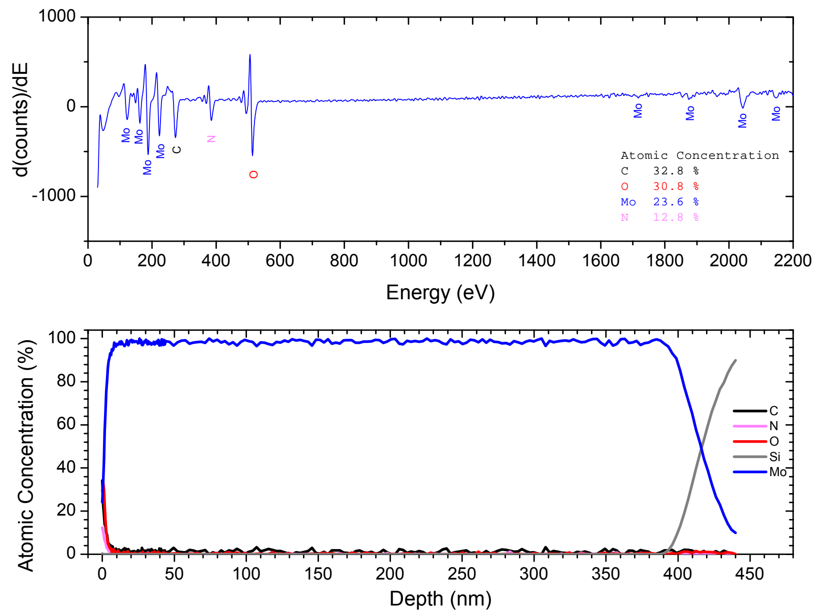

Figure 14. AES data for the LPP-exposed Mo sample

The data shown in Figure 13 and Figure 14 for AES, and Figure 15 and Figure 16 for XPS show that the surfaces were for the most part free of any contaminants. This contrasts with the DPP exposures where we found material from the vacuum chamber (e.g. Fe) and from other samples (Au, Pd, Ru, Mo) redeposited on surfaces. We also found electrode material and xenon implanted in the samples after DPP exposure. Some of this is probably due to the fewer number of shots for the LPP exposures. It is also possible that xenon exists in the LPP-exposed samples, but we were unable to do depth profiling with XPS. Since XPS is much more sensitive to xenon than AES, it is not surprising that we have yet to see evidence of Xe.

Table 6 summarizes any interesting elements found in the samples, i.e. other than C and oxygen which are present on all surfaces. In AES, we saw argon and Si on the C surface before depth profiling would have possibly introduced argon into the sample. Si could possibly have come from other samples or the substrate. AES also showed the presence of N on the Mo surface, which was not seen in XPS.

XPS showed nitrogen on the Au surface, as well as possibly fluorine. A peak near where fluorine's 1s peak would be appeared in the Au, ML1 (Figure 15), and Mo (Figure 16) samples. However evidence of F was not seen in AES (which should be reasonably sensitive), making its presence questionable. In addition, both AES and XPS found traces of Cl and S on the Pd sample.

Table 6. Elements seen (other than the sample material(s), C, and oxygen) in AES and XPS

Sample	AES	XPS
Au		F, N
C	Ar, Si	—
ML1		F
Mo	N	F
Pd	**Cl**, **S**	**Cl**, N, **S**
Ru		
Si		

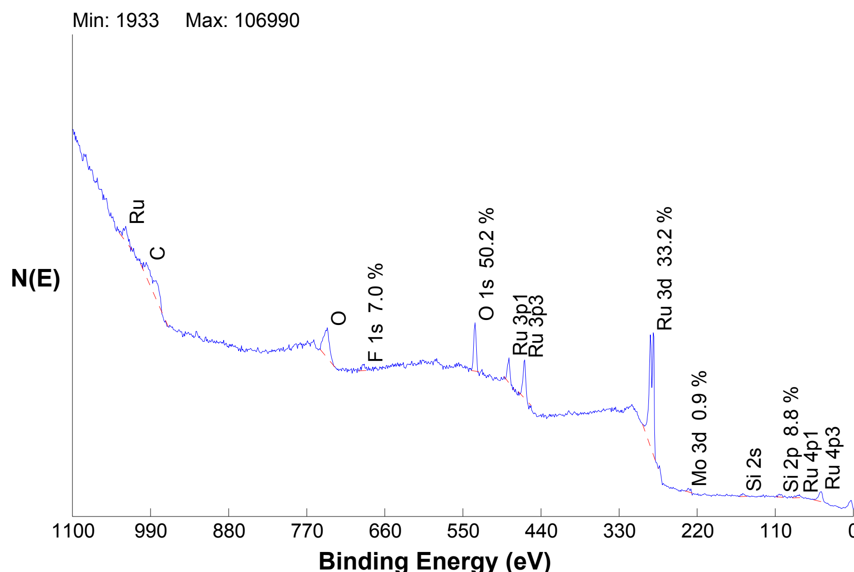

Figure 15. XPS data for the LPP-exposed ML1 sample

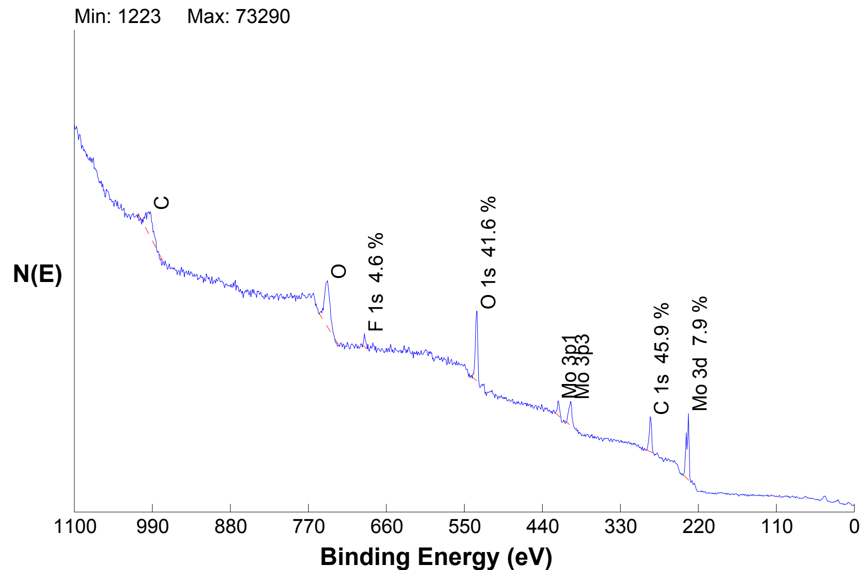

Figure 16. XPS data for the LPP-exposed Mo sample

3. CONCLUSIONS

The seven samples (Au, C, ML1, Mo, Pd, Ru, and Si) exposed in the ETS LPP source at Sandia National Laboratories have been analyzed at the University of Illinois. Samples were exposed to 500,000 shots; twenty times fewer than the initial exposures performed in the XTS DPP source at UIUC. This difference is made up for somewhat by the samples being much closer to the source in the LPP exposures (10-17 cm vs. 56 cm), and the lack of debris mitigation on the LPP source.

Analysis of the LPP-exposed samples, as well as earlier analysis of unexposed samples and a batch exposed in the DPP source, was performed at UIUC's Center for Microanalysis of Materials. Techniques performed included AFM, XRD, XRR, SEM, AES, and XPS. AFM and XRR gave the surface roughness. XRD gave information on the texture of the samples. SEM provided the best estimates of film thickness and erosion. Finally, AES and XPS measured the elemental composition of the samples vs. depth.

Six of the seven samples became rougher after exposure in the LPP source. The increase was between 1.1 and 4.5x. The metals (Au, Mo, Ru, Pd) showed the greatest increase in RMS roughness. C showed a very slight increase, while the multilayer sample appeared smoother after exposure. This could occur if the Ru capping layer had been eroded, exposing a smooth Si layer. There was no definite trend in roughness when comparing the LPP and DPP exposures. In some cases the LPP samples were rougher, and other samples the opposite was true.

The metallic films exhibited a fiber texture, tending to grow up from the substrate in vertical columns. The multilayer, C, and Si films were harder to evaluate. The individual layers of the multilayer are extremely thin, and the Si layers match the substrate. The Si film is probably single crystal, like the substrate. The C film was either too thin to measure well or possibly amorphous. There was some decrease in average grain sizes after exposure, but for the most part XRD on the LPP-exposed samples showed little change from the unexposed or DPP-exposed samples.

In terms of erosion, the LPP samples showed less material removed than the DPP exposures. This is probably due to the shorter duration of exposure. Erosion was estimated to be between 5 nm (for ML1) and 48 nm (for Au). In comparison, the DPP erosion varied from 10 nm (for Mo) to 54 nm (for Au). Several of the samples presented problems in the cross

sectional SEMs, including C, Si, and Ru. Since the erosion was not 20x less than in the DPP exposures, it can be concluded that the erosive ion flux to the samples was larger in the LPP exposures.

The LPP-exposed samples tended to be somewhat “cleaner” than the samples exposed in the DPP. In the DPP exposures, we found various elements deposited on the sample surfaces (Fe, Au, Ru, Mo) and some elements (Xe and electrode materials) deposited deep in the surfaces due to energetic impact. Future XPS depth profiling work may be able to determine more conclusively if debris ions are implanted in the LPP-exposed samples.

ACKNOWLEDGEMENTS

The authors would like to thank project manager Ginger Edwards and support from SEMATECH. Additional assistance from Robert Bristol at Intel Components Research and the Xtreme Technologies GmbH team in Göttingen were wholeheartedly appreciated. A portion of this research was carried out in the Center for Microanalysis of Materials, University of Illinois, which is partially supported by the U.S. Department of Energy under grant DEFG02-91-ER45439.